Atomistic Origin of Photoluminescence Quenching in Colloidal MoS_2 and WS_2 Nanoplatelets

Surender Kumar®,*,†,# Markus Fröhlich®,‡,# Stefan Velja®,† Marco Kögel® ,¶,§

Onno Strolka®,‡,|| André Niebur®,|| Samuell Ginzburg®, Lauthammad Sufyan

Ramzan®,† Jannik C. Meyer®,§,¶ Jannika Lauth®,*,‡,|| and Caterina Cocchi®*,†

†Institut für Festkörpertheorie und -Optik, Friedrich-Schiller-Universität Jena, 07743 Jena,

Germany

‡Institute of Physical and Theoretical Chemistry, Eberhard Karls University of Tübingen,
72076 Tübingen, Germany

¶NMI Natural and Medical Sciences Institute at the University of Tübingen, 72770

Reutlingen, Germany

§University of Tübingen, Institute of Applied Physics, 72076 Tübingen, Germany

||Leibniz University of Hannover, Cluster of Excellence PhoenixD (Photonics, Optics and

Engineering - Innovation Across Disciplines), 30167 Hannover, Germany

\(\perp \text{Yusuf Hamied Department of Chemistry, University of Cambridge, Lensfield Road,}\)

Cambridge, UK

#These authors contributed equally to this work.

E-mail: surendermohinder@gmail.com; jannika.lauth@uni-tuebingen.de; caterina.cocchi@uni-jena.de

Abstract

Large chemical tunability and strong light-matter interactions make colloidal transition metal dichalcogenide (TMD) nanostructures particularly suitable for light-emitting applications. However, ultrafast exciton decay and quenched photoluminescence (PL) limit their potential. Combining femtosecond transient absorption spectroscopy with first-principles calculations on MoS₂ and WS₂ nanoplatelets, we reveal that the observed sub-picosecond exciton decay originates from edge-located optically bright hole traps. These intrinsic trap states stem from the metal d-orbitals and persist even when the sulfur-terminated edges are hydrogen-passivated. Notably, WS₂ nanostructures show more localized and optically active edge states than their MoS₂ counterparts, and zigzag edges exhibit a higher trap density than armchair edges. The nanoplatelet size dictates the competition between ultrafast edge-trapping and slower core-exciton recombination, and the states responsible for exciton quenching enhance catalytic activity. Our work represents an important step forward in understanding exciton quenching in TMD nanoplatelets and stimulates additional research to refine physicochemical protocols for enhanced PL.

Keywords

Transient absorption spectroscopy, photoluminescence quenching, DFT, edge states, MoS_2 and WS_2

Substrate-free colloidal synthesis is a scalable and versatile bottom-up method to produce transition metal dichalcogenide (TMD) nanostructures. ^{1–6} This approach offers thermodynamically stable 2H-phase monolayers ⁵ with lateral sizes down to a few nanometers, ^{4,5,7–9} enabling fine control over composition and surface chemistry. ^{1–5,8,9} Among low-dimensional TMDs, MoS₂ and WS₂ stand out for their direct visible-range bandgaps, strong light-matter coupling, and tunable optical properties, ^{5,10,11,11–22} which makes them highly promising for thin-film integration in optoelectronic devices.

High photoluminescence (PL), long-lived emissive states, and tunable emission spectra are highly desirable properties for light-emitting applications. TMDs exhibit these optimal optical features thanks to their exceptionally bound excitons (~0.5 eV binding energies). ^{21,23} Although excitons are expected to radiatively recombine with high quantum efficiency, ^{24–27} colloidal TMD nanostructures typically show weak or quenched PL ^{28–32} compared to monolayers obtained via exfoliation/chemical vapor deposition (CVD). ^{33–38} This PL loss can originate from non-radiative recombination at surface or edge sites, ^{10–13} charge carrier trapping, ^{14,28,30,31,33,39,40} and chemical passivation of surface states. ^{15,16,41} However, the intrinsically disordered nature of colloidal samples makes it non-trivial to isolate the specific physical contributions. As a result, the fundamental, atomistic origin of PL quenching and charge carrier trapping in colloidal TMD nanostructures remains unclear to date.

Ab initio structure calculations represent a valuable resource to complement structural analysis and spectroscopic characterization of colloidal systems. Density functional theory (DFT) has been successfully applied to determine trap states in III-V and II-VI colloidal nanostructures, ^{42–46} revealing their microscopic origin and electronic character. These exemplary results demonstrate the potential of this parameter-free approach, which can contribute to accurately identify the microscopic origin of PL quenching in colloidal TMD nanostructures, by systematically investigating different compositions, sizes, and terminations with atomistic control.

By combining transient absorption spectroscopy with DFT calculations, we identify edge-

localized metal d-orbitals acting as trap states to be responsible for ultrafast exciton decay in colloidal WS₂ and MoS₂ nanoplatelets (NPLs), driving sub-picosecond PL quenching. Furthermore, we reveal how the optical properties of TMD NPLs evolve with size and how their edge states, while detrimental to PL, are key to their catalytic activity. Our findings establish a clear link between material morphology, fundamental photophysics, and functional performance, providing a rational basis for the design of versatile wet-chemically synthesized TMD nanostructures.

MoS₂ and WS₂ colloidal NPLs and nanosheets (NSs) [Figure 1] are synthesized by dropwise addition of MoCl₅/WCl₆ dissolved in oleylamine (OlAm) into a 320 °C solution of elemental sulfur and hexamethyldisilazane (HMDS) in OlAm. A short addition time of 10 min and using sulfur in excess (\sim 700 equivalents (eq)) limits the lateral growth, resulting in NPLs. A longer addition time and a lower sulfur excess (3.4 eq), on the other hand, yields laterally larger NSs. But to agglomeration caused by solvent evaporation, the NPLs arrange in macroscopic structures, resulting in the observed Moiré patterns. OlAm ligands used in the synthesis ensure the spatial separation of the NPLs/NSs even when agglomerated, as reported previously. Salve WS₂ NPLs have an average lateral size of 3.7 \pm 1.7 nm and NS a size of 21 \pm 5 nm [Figure 1 (c)]. MoS₂ NPLs and NSs [Figure 1 (d)] show similar size values (3.7 \pm 1.6 nm and 20 \pm 4 nm). Both NPLs and NSs show a hexagonal 2H-phase crystal structure, highlighted in the fast Fourier transform (FFT)-inset of Figure 1 (a,b).

Compared to the larger NSs, the reduced size of NPLs introduces additional lateral confinement, which results in a hypsochromic shift and a broadened and decreased excitonic absorption [Figure 2 (a,b)], which is most effective on the A-exciton features. The broad absorption is attributed to a combination of inhomogeneous size broadening and locally different morphologies [Figure 1 (a,b)], since both the relative width of the size distribution and the edge-to-core atom ratio are higher in NPLs than in the NSs.

The reduced absorption is a result of the smaller NPLs size, since the oscillator strength is proportional to the surface dimensions. ^{49–51} In earlier work, some of us have discussed

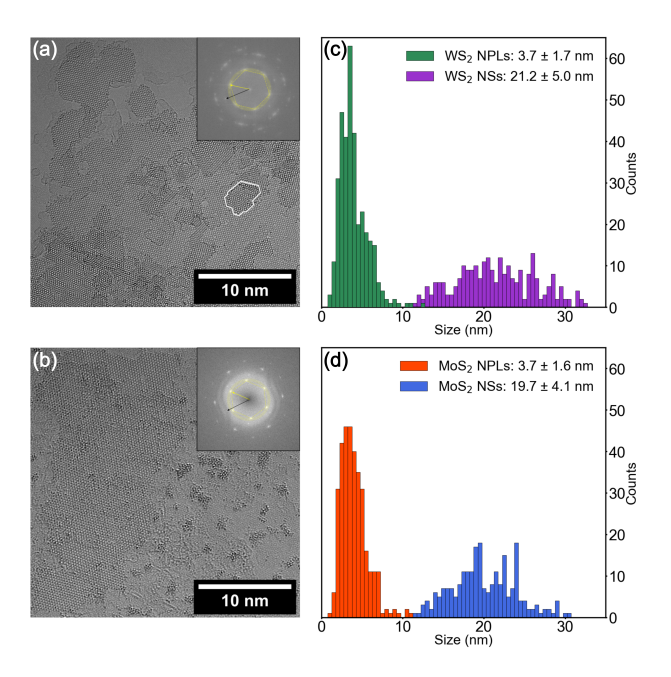


Figure 1: High resolution TEM-image of (a) WS₂ NPLs and (b) MoS₂ NSs, different in shape, size and orientation. A single exemplary NPL is highlighted with a white border. The hexagonal crystal structure of the semiconducting 2H-phase can be seen in the FFT-inset (yellow) with the underlying graphene structure indicated by the black arrow. Size distributions of (c) WS₂, and (d) MoS₂ NPLs and NSs respectively.

the vanishing absorption of the A-excitonic transition in colloidal MoS₂ NPLs, showing that the feature at 2.09 eV (593 nm) belongs to the B-exciton and is shifted to higher energies from 2.03 eV (610 nm) due to the added lateral confinement^{7,28} (see Figure S1). By qualitatively comparing line cuts of the transient absorption (TA) spectra, acquired immediately after photoexcitation [t_0 , Figure 2 (a,b)], we notice that both WS₂ and MoS₂ NPLs behave similarly under lateral confinement, due to a hypsochromic absorption shift, broadening the features and causing a loss of signal. Quantitatively, MoS₂ NPLs show a stronger shift (150 meV, 47 nm) than WS₂ (37 meV, 11 nm), indicating that MoS₂ is more prominently affected by lateral confinement. TA spectra further show the correlation between lateral size and charge carrier dynamics in MoS₂ and WS₂ NPLs and NSs. The A-excitons [Figure 2 (c)] of MoS₂ and WS₂ NPLs (t_1 : 270/291 fs, t_2 : 21/11 ps) exhibit a significantly faster decay than in the larger NSs (t_1 : 410/741 fs, t_2 : 40/29 ps, t_3 : > 7.5 ns, see Table 1).

A rapid, sub-picosecond trapping process is observed in both MoS₂ and WS₂ nanostruc-

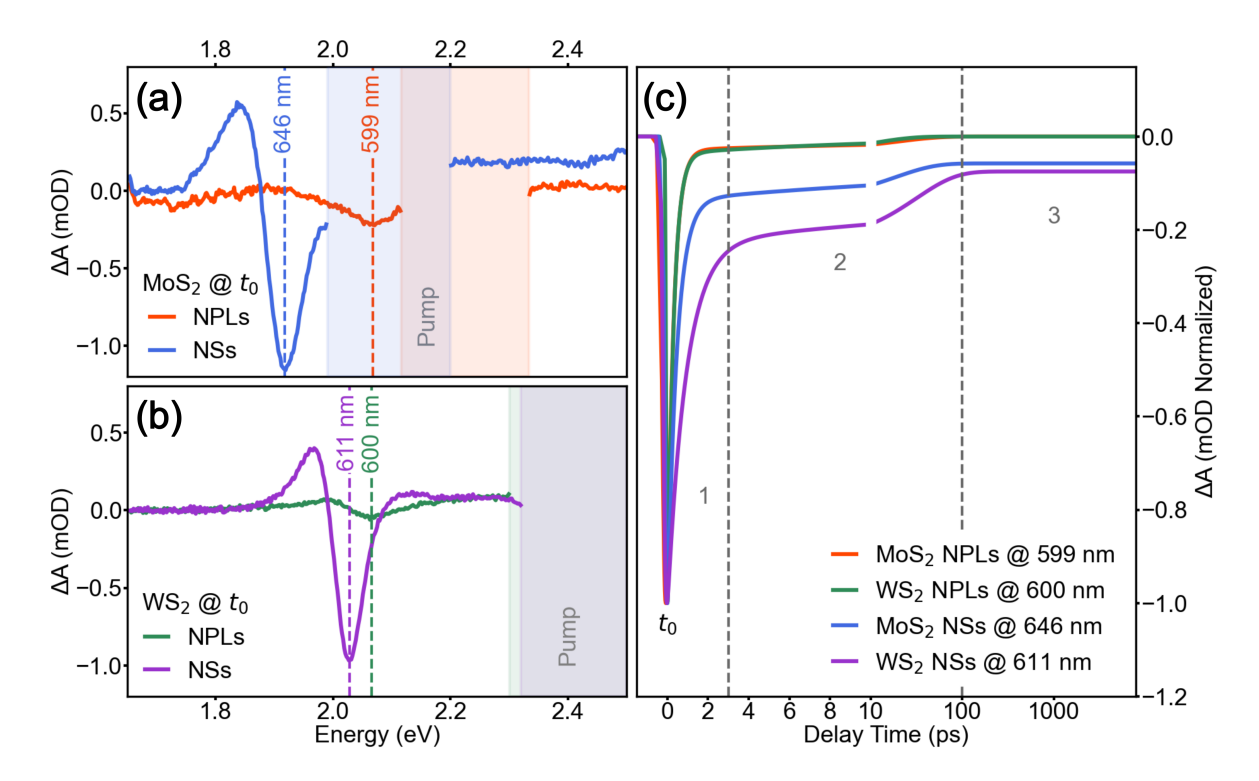


Figure 2: (a, b) Spectral line cuts of MoS_2 (a) and WS_2 (b) at t_0 showcasing shift, broadening and weakening of the A-excitonic transition under lateral confinement. The spectral position of each A-exciton is marked by a vertical line, while the areas obscured by the pump pulse are marked in the resp. color of the corresponding graph. (c) Decay dynamics of the A-exciton of all samples. The time scale is linear between -0.5 and 10 ps and logarithmic from 10-7500 ps to allow both high resolution of the early response and maximum coverage.

tures. However, as shown in Table 1, this effect is more pronounced in the NPLs, being faster and contributing a larger amount to the overall decay. Such a behavior points to a higher density of mid-gap trap states favoring non-radiative decay in NPLs.^{7,28} In monolayer colloidal TMD NSs, electron trapping mechanisms have been linked to sulfur vacancies, ³⁰ while hole trapping was reported for multilayered NSs.³¹ However, these similar decay mechanisms cannot be directly translated to interpret the results obtained for relatively smaller MoS₂ and WS₂ NPLs. In NPLs, the reduced lateral size leads to a significantly higher density of exposed edge sites compared to NSs. Consequently, different mechanisms may emerge, exclusively shaping the exciton decay in these edge-dominated structures. While both nanostructures show picosecond bathochromic shifts of absorption (positive signal at lower energies for each exciton bleach in Figure S2) consistent with band gap renormaliza-

Table 1: Decay times fitted by a sequential bi/tri-exponential model for initial carrier trapping t_1 , band gap renormalization t_2 , and slow recombination from trapped states t_3 of MoS₂ and WS₂ NPLs and NSs extracted from the global analysis using TAPAS ⁵² (described in the supporting info).

	$\mathbf{t_1}$	t_2	t_3
MoS_2 NPLs	$(270 \pm 50) \text{ fs}$	$(21 \pm 7) \text{ ps}$	_
$MoS_2 NSs$	$(410 \pm 100) \text{ fs}$	$(40 \pm 7) \text{ ps}$	$\rightarrow \infty$
WS ₂ NPLs	$(291 \pm 40) \text{ fs}$	$(11 \pm 1) \text{ ps}$	-
$WS_2 NSs$	$(741 \pm 40) \text{ fs}$	$(29 \pm 2) \text{ ps}$	$\rightarrow \infty$

tion, ^{7,28,53} a distinct, long-lived process [Figure 2 (c)], likely bright exciton recombination, is observed exclusively in NSs. ^{29,32,48} Although our temporal measurements suggest the involvement of mid-gap states in NPLs, the decay data alone are insufficient to conclusively assign their structural or chemical origin.

To understand the mid-gap states inferred from our time-resolved spectroscopic measurements, we perform DFT calculations to investigate the electronic structure of a series of MoS₂ and WS₂ NPLs. Our model structures [Figure 3 (a)] are monolayer-thick pseudo-hexagonal 2H-polymorphic NPLs with varying lateral dimensions of 0.9, 1.5, and 2.1 nm. These model structures are qualitatively representative of the experimental NPLs reported in Figure 1 (a). Their size falls in the experimental range, which is reasonable for rationalizing the measurements. The optimized geometries are defect-free and fully passivated, featuring zigzag (ZZ, edge S-atoms bonded to two Mo (W) atoms) and armchair (AC, edge S-atoms bonded to a single Mo (W) atom) edges. Hydrogen passivation effectively removes under-coordinated surface S-atoms and can exist in experiments. ^{54–58} The formation energy [Figure 3 (b)] decreases as both MoS₂ and WS₂ NPL size grows. This trend is consistent with the size distribution observed in our measurements [Figure 1 (c)] and reflects the enhanced thermodynamic stability of larger NPLs. At comparable sizes, WS₂ NPLs are consistently more stable than MoS₂, due to the stronger bonds and higher ionic character of W-S relative to Mo-S bond. ⁵⁹

To verify whether trap states are present in the NPLs, we investigate the electronic

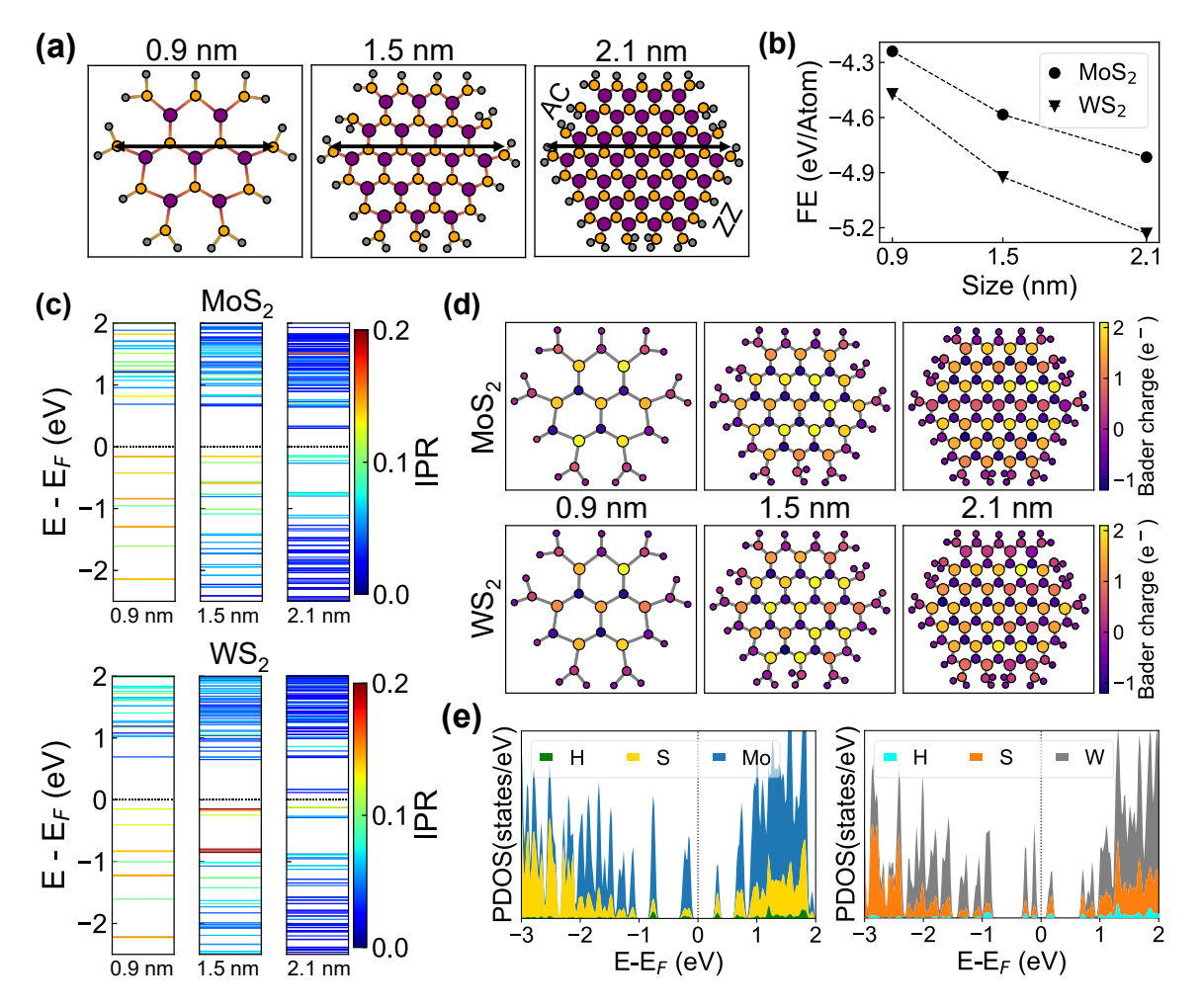


Figure 3: (a) Optimized structures of hydrogen-passivated MoS_2 nanoplatelets (NPLs) of different sizes with zigzag (ZZ)and armchair (AC) S-edges. Mo atoms are shown in purple, S in yellow, and H in gray. Black arrows indicate the size. (b) Formation energies of MoS_2 and WS_2 NPLs as a function of size. (c) Inverse participation ratio for states around Fermi energy (E_F) for MoS_2 and WS_2 NPLs. (d) Net Bader charges for calculated MoS_2 (top) and WS_2 (bottom) NPL sizes. (e) Projected density of states (PDOS) near the Fermi level for 2.1 nm MoS_2 (left) and WS_2 (right) NPLs.

structure [Figure 3 (c)] near the Fermi level (E_F). Both MoS₂ and WS₂ NPLs show a semiconducting behavior with a band gap decreasing as the NPL size increases, following the expected trend of quantum confinement. The single-particle-state analysis based on the inverse participation ratio 46,60,61 [IPR, Figure 3 (c)], a standard metric to assess wavefunction localization, 62,63 we find that several hole (occupied) states near E_F in both WS₂ and MoS₂ have high IPR values across all considered sizes, indicating a strong localization. In the smallest structures (0.9 nm) of both materials, most hole states are relatively localized compared to the largest NPL (2.1 nm). Conversely, the deeper occupied states become increasingly delocalized, approaching a bulk-like character. This trend is a size effect, resulting from the decreased relative number of edge atoms in larger flakes. In contrast, the electron (unoccupied) states remain largely delocalized, with only occasional localized states in the largest MoS_2 and WS_2 NPLs. Notably, WS_2 NPLs show more localized states near E_F than MoS_2 , which correlates with the differences in the temporal measurements.

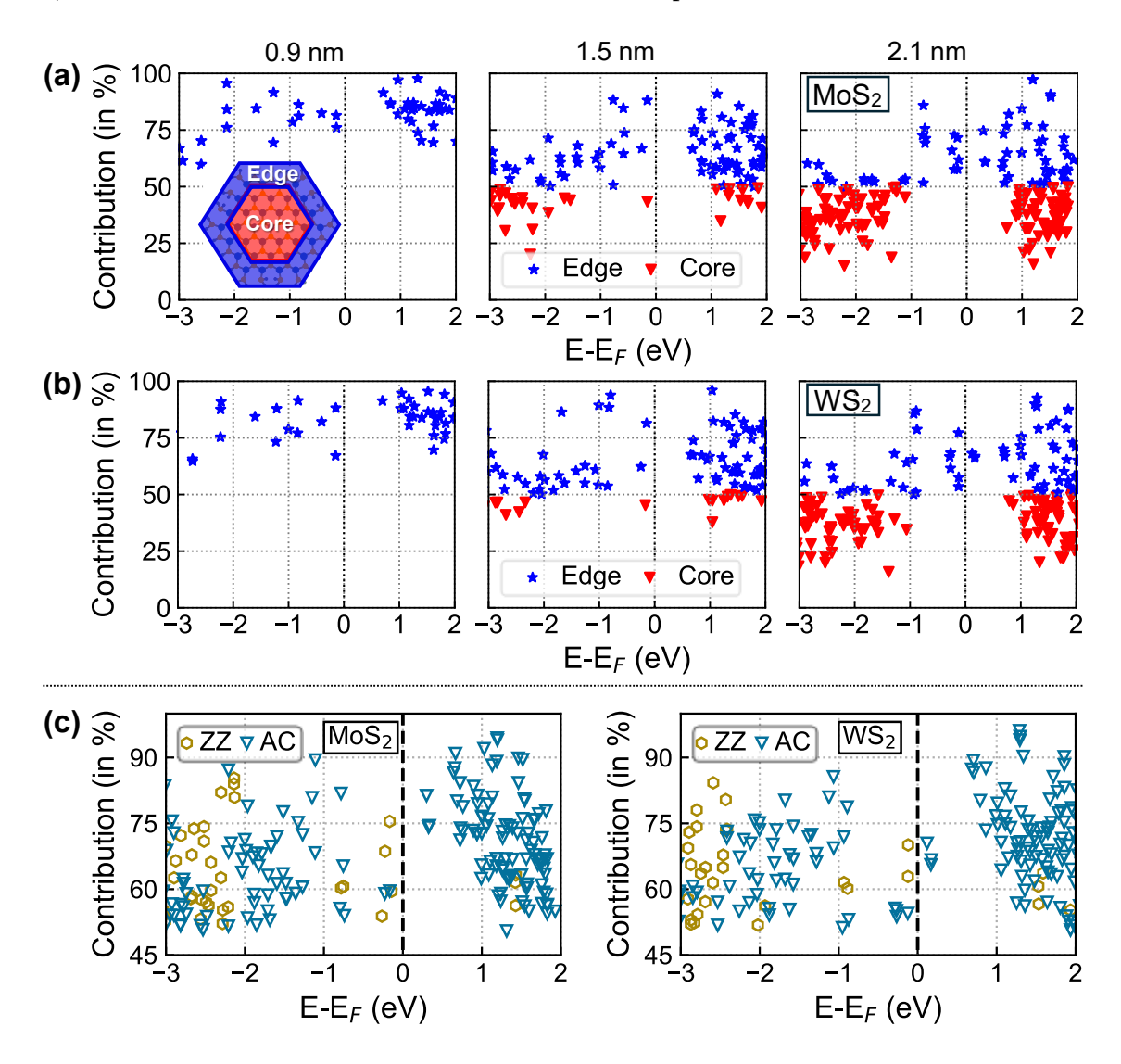


Figure 4: Calculated core-edge contributions to energy levels near the Fermi energy in (a) MoS_2 and (b) WS_2 NPLs. Blue stars (red triangles) mark states with > 50% edge (core) contribution for the core-edge partitioning. (c) Relative contributions of zigzag (ZZ) and armchair (AC) edges to electronic states near the Fermi energy (E_F) in 2.1 nm MoS_2 (left) and (b) WS_2 (right) NPLs.

To analyze the origin of electronic state localization, we perform Bader charge analysis of local charge fluctuations in the considered structures [Figure 3 (d)]. Each NPL has a uniform core and a chemically distinct edge (Mo-S-H or W-S-H), with charge deviations increasing in larger flakes [Figure 3 (d)]. In the central region, electron transfer from Mo (or W) to S occurs, consistent with their different electronegativity. At the edges, disrupted bonding reduces the ability of atoms to fully share or accept electrons and breaks the local lattice periodicity, giving rise to spatially localized electronic states |Figure 4 (c)| near E_F . Despite S-termination and H-passivation, edge metal atoms dominate the charge distribution, indicating their major role in the localized states. Different charge fluctuation patterns emerge in MoS₂ and WS₂ NPLs of equal size. The central metal atoms in WS₂ display a more uniform charge distribution, in contrast to the uneven charge distribution in MoS₂, which also leads to charge differences at the edges. Moreover, in both materials, S atoms along ZZedges are more negatively charged than along AC-edges [Figure 3 (d)], suggesting preferential ligand sites for edge-specific passivation. The projected density of states (PDOS) of MoS₂ and WS₂ NPLs provides additional information about the orbital contributions to the energy levels. As shown in Figure 3 (e) for the systems with 2.1 nm size, the hole (occupied) states up to about 2 eV below the Fermi level are dominated by metal d-orbitals (Figure S5), while S p-orbitals contribute deeper in energy, although signs of hybridization are present everywhere. In the electron (unoccupied) region, the trend does not change significantly, with the metal d-orbitals remaining predominant in the considered energy range. Here, hydrogen states contribute more than in the hole region.

We complete our analysis by inspecting the contributions from the interior (core) and exterior (edge) region of the considered NPLs [Figure 4]. Specifically, we identify the origin of a specific state if more than 50% of its contributions come from either portion of the nanostructure. Across all structures and in both compositions, both hole and electron states near E_F are predominantly edge-localized across all sizes of MoS_2 and WS_2 [Figure 4 (a,b)]. In the smallest flake (0.9 nm), where nearly all atoms lie at the periphery, all states obviously

originate from the edges. As the flake size increases, core-localized states gradually emerge; however, even in the largest flake (2.1 nm), states within ~ 1 eV of the Fermi level remain mostly edge-localized.

For the largest 2.1 nm NPLs, we additionally investigate the contributions of states belonging to each edge type [Figure 4 (c)]. Near E_F in the occupied region, states on zigzag edges contribute slightly more than those on armchair edges, while deeper hole states show increasing contributions from armchair edges. Electron states up to \sim 1 eV are mostly dominated by armchair-edges contributions in both MoS_2 and WS_2 NPLs. This edge-dependent behavior, characterized by localized states and charge imbalances, establishes the edges as chemically active sites. These findings thus explain why MoS_2 and WS_2 nanostructures are highly effective in photocatalysis. $^{64-71}$

To gain qualitative insight into the optical activity of the investigated NPLs, we calculate the normalized oscillator strengths within the independent-particle approximation (IPA), see Figure 5. Consistent with the prevalence of edge states in the gap region of both WS₂ and MoS₂ NPLs, the lowest-energy transitions primarily involve edge-localized states, with no core-originated transitions appearing below 4 eV in the spectrum of the smallest flake (0.9 nm). As the flake size increases to 2.1 nm, core-localized transitions progressively emerge but they remain systematically higher in energy compared to the edge-localized excitations, in agreement with the localization of the electronic states near the Fermi energy. While in both MoS₂ and WS₂ 1.5 nm NPLs manifolds of weak core-originate transitions appear in Figure 5 (a,b), in the nanostructures with 2.1 nm radius, the density of these excited states and their relative strength increases dramatically, contributing substantially to the optical activities of both NPLs above 2 eV.

These findings suggest that core-originated transitions will dominate over edge transitions in larger NSs, leading to longer-lived exciton decay, ²⁸ consistent with the measured decay times summarized in Table 1. Direct comparison of MoS₂ and WS₂ NPLs reveals markedly enhanced edge-state emission in WS₂. In 2.1 nm WS₂, the edge-originated excited states at

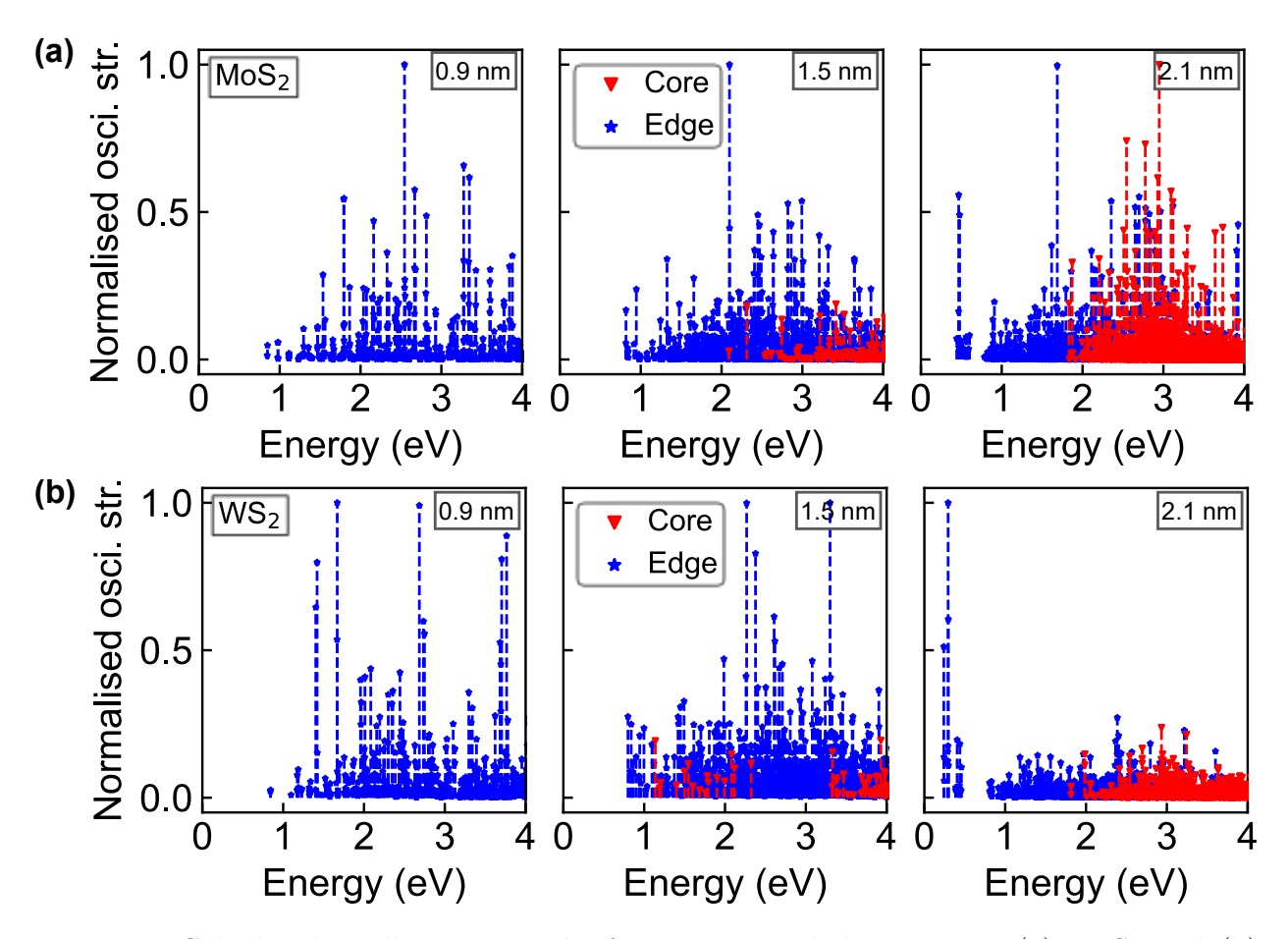


Figure 5: Calculated oscillator strengths for transitions below 4 eV in (a) MoS_2 and (b) WS_2 NPLs, colored based on state character: red (core-originated, both states < 50% edge character), blue (edge-originated, at least one state has > 50% edge character).

the spectral onset (0.2–0.5 eV) are \sim 10 orders of magnitude brighter than the higher-energy core transitions, while in MoS₂, the relative intensity of the two manifolds is comparable. This striking contrast signifies stronger optical coupling and radiative recombination in WS₂, consistent with our measurements. In MoS₂ on the other hand, the comparable core- and edge-state intensities promote state hybridization and non-radiative quenching, which also agrees with the findings. Furthermore, our work contextualizes different carrier trapping as compared to larger TMD nanosheets.³⁰ In MoS₂ and WS₂ NPLs, we identify that lateral edges control the optical response which host optically bright hole traps (majorly) from highly localized Mo/W d-orbitals. Notably, these bright edge-hosted traps persist even in the absence of vacancy defects that are known to induce non-radiative electron trapping in

extended TMD sheets.³⁰ Hence, reducing the lateral dimensions reshapes the trap landscape observed in NSs, favoring hole over electron trapping and inducing the observed ultrafast radiative recombination.

In summary, this study offers a comprehensive understanding of the exciton dynamics in colloidal WS₂ and MoS₂ NPLs, revealing the atomistic origin of their quenched PL. We demonstrate edge-located hole traps to explain the ultrafast sub-picosecond exciton decay in laterally confined TMD NPLs, even without the introduction of sulfur vacancies. Our combined experimental and theoretical approach, identifies these traps as optically bright. With increasing NPL size, the core steadily dominates, reducing the contribution of edge states and resulting in longer-lived exciton decay, consistent with our experimental observations on NSs. Furthermore, a high density of localized states at the edges enables efficient charge transfer. This explains the exceptional photocatalytic activity of TMD nanostructures.

Our work unravels not only the fundamental physics behind exciton quenching in colloidal TMDs but also opens a pathway for future design strategies, like post-synthesis chemical treatment or functionalization, to optimize the optical behavior of these systems. With the gained understanding of the importance of metal d-states and their influence of NPL size and edge shape, we can now explore new avenues to enhance PL quantum efficiency and catalytic performance. We anticipate that the trap states predicted here should also manifest in other TMD nanostructures. Future work based on advanced many-body calculations will provide a quantitative characterization of the exciton states and their dynamics, while the inclusion of explicit ligands will improve our understanding of the impact of functionalization on PL efficiency.

Acknowledgement

CC acknowledges support from the DFG Collaborative Research Center 1375, project no. 398816777, subproject A08. SV and CC acknowledge funding from the QuantERA II pro-

gram under the European Union's Horizon 2020 research and innovation program, within the EQUAISE project (Grant Agreement no. 101017733). SG acknowledges support from the Humboldt Internship Program. JL acknowledges funding of the TA measurements by the DFG under contract INST 37/1160-1 FUGG (project nr. 458406921), and gratefully acknowledges additional funding by the DFG under the Excellence Strategy of the Cluster of Excellence PhoenixD (EXC 2122, Project ID 390833453) and by an Athene Grant of the University of Tübingen (by the Federal Ministry of Education and Research (BMBF) and the Baden-Württemberg Ministry of Science as part of the Excellence Strategy of the German Federal and State Governments). JCM and MK acknowledge funding from the German Research Foundation (DFG), project ME 3313/6-1, by the Ministry of Science, Research and Art Baden-Württemberg, Germany and by the European Union under EU-EFRE grant no. 712889.

Potential Reviewer List

- Iwan Moreels, Iwan.Moreels@UGent.be
- Shalini Singh, Shalini.Singh@ul.ie
- Benoit Mahler, benoit.mahler@univ-lyon1.fr
- Jan-Ole Joswig jan-ole.joswig@tu-dresden.de
- Prof. Dr. Laurens Siebbeles L.D.A.Siebbeles@tudelft.nl

Supporting Information Available

The following files are available free of charge.

• si.pdf: The supporting information includes: Experimental and computational method details; structural properties, element and orbital resolved PDOS for all structures from

main text.

Data Availability Statement

Input and output files of the ab initio calculations performed in this work are available free of charge in Zenodo DOI: 10.5281/zenodo.17661456 [record: 17661456]. Experimental data is available from the corresponding author JL upon reasonable request.

Notes

The authors declare no competing financial interest.

References

- (1) Mahler, B.; Hoepfner, V.; Liao, K.; Ozin, G. A. Colloidal Synthesis of 1T-WS₂ and 2H-WS₂ Nanosheets: Applications for Photocatalytic Hydrogen Evolution. J. Am. Chem. Soc. 2014, 136, 14121–14127.
- (2) Sun, Y.; Fujisawa, K.; Lin, Z.; Lei, Y.; Mondschein, J. S.; Terrones, M.; Schaak, R. E. Low-Temperature Solution Synthesis of Transition Metal Dichalcogenide Alloys with Tunable Optical Properties. J. Am. Chem. Soc. 2017, 139, 11096–11105.
- (3) Sun, Y.; Terrones, M.; Schaak, R. E. Colloidal Nanostructures of Transition-Metal Dichalcogenides. Acc. Chem. Res. 2021, 54, 1517–1527.
- (4) Chen, C.; Qiao, H.; Lin, S.; Man Luk, C.; Liu, Y.; Xu, Z.; Song, J.; Xue, Y.; Li, D.; Yuan, J.; Yu, W.; Pan, C.; Ping Lau, S.; Bao, Q. Highly Responsive MoS₂ Photodetectors Enhanced by Graphene Quantum Dots. *Sci. Rep.* **2015**, *5*, 11830.
- (5) Zechel, F.; Hutár, P.; Vretenár, V.; Végsö, K.; Šiffalovič, P.; Sýkora, M. Green Colloidal Synthesis of MoS₂ Nanoflakes. *Inorg. Chem* **2023**, *62*, 16554–16563.

- (6) Kapuria, N.; Patil, N. N.; Sankaran, A.; Laffir, F.; Geaney, H.; Magner, E.; Scanlon, M.; Ryan, K. M.; Singh, S. Engineering Polymorphs in Colloidal Metal Dichalcogenides: Precursor-Mediated Phase Control, Molecular Insights into Crystallisation Kinetics and Promising Electrochemical Activity. J. Mater. Chem. A 2023, 11, 11341–11353.
- (7) Niebur, A.; Söll, A.; Haizmann, P.; Strolka, O.; Rudolph, D.; Tran, K.; Renz, F.; Frauendorf, A. P.; Hübner, J.; Peisert, H.; Scheele, M.; Lauth, J. Untangling the Intertwined: Metallic to Semiconducting Phase Transition of Colloidal MoS₂ Nanoplatelets and Nanosheets. *Nanoscale* **2023**, *15*, 5679–5688.
- (8) Fröhlich, M.; Kögel, M.; Hiller, J.; Kahlmeyer, L.; Meixner, A. J.; Scheele, M.; Meyer, J. C.; Lauth, J. Colloidal 2D Mo_{1-x}W_xS₂ Nanosheets: An Atomic- to Ensemble-level Spectroscopic Study. Phys. Chem. Chem. Phys. 2024, 26, 13271–13278.
- (9) Joseph, S.; Mohan, J.; Lakshmy, S.; Thomas, S.; Chakraborty, B.; Thomas, S.; Kalarikkal, N. A Review of the Synthesis, Properties, and Applications of 2D Transition Metal Dichalcogenide and their Heterostructures. *Mater. Chem. Phys.* 2023, 297, 127332.
- (10) Gopalakrishnan, D.; Damien, D.; Li, B.; Gullappalli, H.; Pillai, V. K.; Ajayan, P. M.; Shaijumon, M. M. Electrochemical Synthesis of Luminescent MoS₂ Quantum Dots. *Chem. Commun.* **2015**, *51*, 6293–6296.
- (11) Wang, X.; Sun, G.; Li, N.; Chen, P. Quantum Dots Derived from Two-dimensional Materials and their Applications for Catalysis and Energy. Chem. Soc. Rev. 2016, 45, 2239–2262.
- (12) Nguyen, V.; Dong, Q.; Yan, L.; Zhao, N.; Le, P. H. Facile Synthesis of Photoluminescent MoS₂ and WS₂ Quantum Dots with Strong Surface-state Emission. J. Lumin. 2019, 214, 116554.

- (13) Golovynskyi, S.; Bosi, M.; Seravalli, L.; Li, B. MoS₂ Two-dimensional Quantum Dots with Weak Lateral Quantum Confinement: Intense Exciton and Trion Photoluminescence. Surf. Interfaces 2021, 23, 100909.
- (14) Doolen, R.; Laitinen, R.; Parsapour, F.; Kelley, D. F. Trap State Dynamics in MoS₂ Nanoclusters. J. Phys. Chem. B **1998**, 102, 3906–3911.
- (15) Gan, Z. X.; Liu, L. Z.; Wu, H. Y.; Hao, Y. L.; Shan, Y.; Wu, X. L.; Chu, P. K. Quantum Confinement Effects across Two-dimensional Planes in MoS₂ Quantum Dots. Appl. Phys. Lett. 2015, 106, 233113.
- (16) Li, B.; Jiang, L.; Li, X.; Ran, P.; Zuo, P.; Wang, A.; Qu, L.; Zhao, Y.; Cheng, Z.; Lu, Y. Preparation of Monolayer MoS₂ Quantum Dots using Temporally Shaped Femtosecond Laser Ablation of Bulk MoS₂ Targets in Water. Sci. Rep. 2017, 7, 11182.
- (17) Pallikkarathodi Mani, N.; Cyriac, J. Hydrothermal Synthesis of WS₂ Quantum Dots and their Application as a Fluorescence Sensor for the Selective Detection of 2,4,6trinitrophenol. New J. Chem. 2020, 44, 10840–10848.
- (18) Yin, W.; Bai, X.; Chen, P.; Zhang, X.; Su, L.; Ji, C.; Gao, H.; Song, H.; Yu, W. W. Rational Control of Size and Photoluminescence of WS₂ Quantum Dots for White Light-Emitting Diodes. ACS Appl. Mater. Interfaces 2018, 10, 43824–43830.
- (19) Chiu, C.-H.; Chen, Y.-T.; Shen, J.-L. Quantum Dots Derived from Two-dimensional Transition Metal Dichalcogenide: Synthesis, Optical Properties and Optoelectronic Applications. *Nanotechnology* **2023**, *34*, 482001.
- (20) Bertram, N.; Cordes, J.; Kim, Y.; Ganteför, G.; Gemming, S.; Seifert, G. Nanoplatelets Made from MoS₂ and WS₂. Chem. Phys. Lett. **2006**, 418, 36–39.
- (21) Mak, K. F.; Lee, C.; Hone, J.; Shan, J.; Heinz, T. F. Atomically Thin MoS₂: A New Direct-gap Semiconductor. *Physical Review Lett.* **2010**, *105*, 136805.

- (22) Wang, Q. H.; Kalantar-Zadeh, K.; Kis, A.; Coleman, J. N.; Strano, M. S. Electronics and Optoelectronics of Two-dimensional Transition Metal Dichalcogenides. *Nature Nanotechnology* **2012**, *7*, 699–712.
- (23) Chernikov, A.; Berkelbach, T. C.; Hill, H. M.; Rigosi, A.; Li, Y.; Aslan, B.; Reichman, D. R.; Hybertsen, M. S.; Heinz, T. F. Exciton Binding Energy and Nonhydrogenic Rydberg Series in Monolayer WS₂. *Phys. Rev. Lett.* **2014**, *113*, 076802.
- (24) Brokmann, X.; Coolen, L.; Dahan, M.; Hermier, J. P. Measurement of the Radiative and Nonradiative Decay Rates of Single CdSe Nanocrystals through a Controlled Modification of their Spontaneous Emission. *Phys. Rev. Lett.* **2004**, *93*, 107403.
- (25) Nirmal, M.; Dabbousi, B. O.; Bawendi, M. G.; Macklin, J. J.; Trautman, J. K.; Harris, T. D.; Brus, L. E. Fluorescence Intermittency in Single Cadmium Selenide Nanocrystals. *Nature* 1996, 383, 802–804.
- (26) Durisic, N.; Wiseman, P. W.; Grütter, P.; Heyes, C. D. A Common Mechanism Underlies the Dark Fraction Formation and Fluorescence Blinking of Quantum Dots. ACS Nano 2009, 3, 1167–1175.
- (27) Banin, U.; Bruchez, M.; Alivisatos, A. P.; Ha, T.; Weiss, S.; Chemla, D. S. Evidence for a Thermal Contribution to Emission Intermittency in Single CdSe/CdS Core/shell nanocrystals. J. Chem. Phys. 1999, 110, 1195–1201.
- (28) Frauendorf, A. P.; Niebur, A.; Rudolph, D.; Oestreich, M.; Lauth, J.; Hübner, J. Ultrafast Recombination Dynamics under Lateral Confinement and Cryogenic Temperatures in Colloidal MoS₂. J. Phys. Chem. C **2024**, 128, 16597–16606.
- (29) Pippia, G.; Rousaki, A.; Barbone, M.; Billet, J.; Brescia, R.; Polovitsyn, A.; Martín-García, B.; Prato, M.; De Boni, F.; Petrić, M. M.; Ben Mhenni, A.; Van Driessche, I.; Vandenabeele, P.; Müller, K.; Moreels, I. Colloidal Continuous Injection Synthesis of

- Fluorescent MoX_2 (X = S, Se) Nanosheets as a First Step Toward Photonic Applications. *ACS Appl. Nano Mater.* **2022**, *5*, 10311–10320.
- (30) Mutyala, C. S.; Pippia, G.; Tanghe, I.; Martín-García, B.; Rousaki, A.; Vanden-abeele, P.; Schiettecatte, P.; Moreels, I.; Geiregat, P. Charge Carrier Dynamics in Colloidally Synthesized Monolayer MoX₂ Nanosheets. J. Phys. Chem. Lett. 2023, 14, 2620–2626.
- (31) Schiettecatte, P.; Geiregat, P.; Hens, Z. Ultrafast Carrier Dynamics in Few-Layer Colloidal Molybdenum Disulfide Probed by Broadband Transient Absorption Spectroscopy. J. Phys. Chem. C 2019, 123, 10571–10577.
- (32) Zhao, Y.; Fröhlich, M.; Kögel, M.; Strolka, O.; Niebur, A.; Parker, T.; Schneider, F.; Meixner, A. J.; Meyer, J. C.; Zhang, D.; Lauth, J. Second-harmonic Generation and Photoluminescence Properties of Colloidal WS₂ Monolayers Deposited from Solution. Nanoscale Horiz. 2025, 10, 3469 – 3477.
- (33) Cunningham, P. D.; McCreary, K. M.; Hanbicki, A. T.; Currie, M.; Jonker, B. T.; Hayden, L. M. Charge Trapping and Exciton Dynamics in Large-Area CVD Grown MoS₂. J. Phys. Chem. C 2016, 120, 5819–5826.
- (34) Li, H.; Wu, J.; Yin, Z.; Zhang, H. Preparation and Applications of Mechanically Exfoliated Single-layer and Multilayer MoS₂ and WSe₂ Nanosheets. Acc. Chem. Res. 2014, 47, 1067–1075.
- (35) Eda, G.; Yamaguchi, H.; Voiry, D.; Fujita, T.; Chen, M.; Chhowalla, M. Photoluminescence from Chemically Exfoliated MoS₂. *Nano Lett.* **2011**, *11*, 5111–5116.
- (36) Nicolosi, V.; Chhowalla, M.; Kanatzidis, M. G.; Strano, M. S.; Coleman, J. N. Liquid Exfoliation of Layered Materials. *Science* **2013**, *340*, 1226419.

- (37) Lee, Y.-H.; Zhang, X.-Q.; Zhang, W.; Chang, M.-T.; Lin, C.-T.; Chang, K.-D.; Yu, Y.-C.; Wang, J. T.-W.; Chang, C.-S.; Li, L.-J.; Lin, T.-W. Synthesis of Large-Area MoS₂ Atomic Layers with Chemical Vapor Deposition. *Adv. Mater.* **2012**, *24*, 2320–2325.
- (38) Zhao, W.; Ghorannevis, Z.; Chu, L.; Toh, M.; Kloc, C.; Tan, P.-H.; Eda, G. Evolution of Electronic Structure in Atomically Thin Sheets of WS₂ and WSe₂. *ACS Nano* **2013**, 7, 791–797.
- (39) Mukherjee, S.; NM, A. K.; Mondal, A.; Mahalingam, V.; Kamaraju, N. Trapping and Exciton-Exciton Annihilation Assisted Ultrafast Carrier Dynamics in Nanosheets of 2H–MoSe₂ and Cr Doped 1T/2H–MoSe₂. J. Chem. Phys. 2023, 159, 164705.
- (40) Wang, H.; Strait, J. H.; Zhang, C.; Chan, W.; Manolatou, C.; Tiwari, S.; Rana, F. Fast Exciton Annihilation by Capture of Electrons or Holes by Defects via Auger Ccattering in Monolayer Metal Dichalcogenides. *Phys. Rev. B* 2015, *91*, 165411.
- (41) Zhang, S.; Hill, H. M.; Moudgil, K.; Richter, C. A.; Hight Walker, A. R.; Barlow, S.; Marder, S. R.; Hacker, C. A.; Pookpanratana, S. J. Controllable, Wide-Ranging n-Doping and p-Doping of Monolayer Group 6 Transition-Metal Disulfides and Diselenides. Adv. Mater. 2018, 30, 1802991.
- (42) Houtepen, A. J.; Hens, Z.; Owen, J. S.; Infante, I. On the Origin of Surface Traps in Colloidal II–VI Semiconductor Nanocrystals. *Chem. Mater.* **2017**, *29*, 752–761.
- (43) Giansante, C.; Infante, I. Surface Traps in Colloidal Quantum Dots: A Combined Experimental and Theoretical Perspective. J. Phys. Chem. Lett. 2017, 8, 5209–5215.
- (44) Kirkwood, N.; Monchen, J. O. V.; Crisp, R. W.; Grimaldi, G.; Bergstein, H. A. C.; du Fossé, I.; van der Stam, W.; Infante, I.; Houtepen, A. J. Finding and Fixing Traps in II–VI and III–V Colloidal Quantum Dots: The Importance of Z-Type Ligand Passivation. J. Am. Chem. Soc. 2018, 140, 15712–15723.

- (45) Alexander, E.; Kick, M.; McIsaac, A. R.; Van Voorhis, T. Understanding Trap States in InP and GaP Quantum Dots through Density Functional Theory. *Nano Lett.* 2024, 24, 7227–7235.
- (46) Kumar, S.; Cocchi, C.; Steenbock, T. Surface Defects and Symmetry Breaking Impact on the Photoluminescence of InP Quantum Dots. *Nano Lett.* **2025**, *25*, 10588–10593.
- (47) Pippia, G.; Van Hamme, D.; Martín-García, B.; Prato, M.; Moreels, I. A Colloidal Route to Semiconducting Tungsten Disulfide Nanosheets with Monolayer Thickness. Nanoscale 2022, 14, 15859–15868.
- (48) Frauendorf, A. P.; Niebur, A.; Harms, L.; Shree, S.; Urbaszek, B.; Oestreich, M.; Hübner, J.; Lauth, J. Room Temperature Micro-Photoluminescence Studies of Colloidal WS₂ Nanosheets. J. Phys. Chem. C 2021, 125, 18841–18848.
- (49) Fouladi-Oskouei, J.; Shojaei, S.; Liu, Z. Robust Tunable Excitonic Features in Monolayer Transition Metal Dichalcogenide Quantum Dots. J. Phys. Condens. Matter. 2018, 30, 145301.
- (50) Ayari, S.; Quick, M. T.; Owschimikow, N.; Christodoulou, S.; Bertrand, G. H. V.; Artemyev, M.; Moreels, I.; Woggon, U.; Jaziri, S.; Achtstein, A. W. Tuning Trion bBinding Energy and Oscillator Strength in a Laterally Finite 2D System: CdSe Nanoplatelets as a Model System for Trion Properties. *Nanoscale* **2020**, *12*, 14448–14458.
- (51) Rodà, C.; Geiregat, P.; Di Giacomo, A.; Moreels, I.; Hens, Z. Area-Independence of the Biexciton Oscillator Strength in CdSe Colloidal Nanoplatelets. *Nano Lett.* 2022, 22, 9537–9543.
- (52) Frech, P.; Scheele, M. TAPAS: Transient Absorption Processing & Analysis Software. ChemRxiv. 2025, This content is a preprint and has not been peer—reviewed.

- (53) Pogna, E. A. A.; Marsili, M.; De Fazio, D.; Dal Conte, S.; Manzoni, C.; Sangalli, D.; Yoon, D.; Lombardo, A.; Ferrari, A. C.; Marini, A.; Cerullo, G.; Prezzi, D. Photo-Induced Bandgap Renormalization Governs the Ultrafast Response of Single-Layer MoS₂. ACS Nano 2016, 10, 1182–1188.
- (54) Sharifvaghefi, S.; Yang, B.; Zheng, Y. New insights on the role of H₂S and Sulfur Vacancies on Dibenzothiophene hydrodesulfurization over MoS₂ Edges. *Appl. Catal. A:* Gen. **2018**, 566, 164–173.
- (55) Lauritsen, J. V.; Nyberg, M.; Vang, R. T.; Bollinger, M. V.; Clausen, B. S.; Topsøe, H.; Jacobsen, K. W.; Lægsgaard, E.; Nørskov, J. K.; Besenbacher, F. Chemistry of Onedimensional Metallic Edge States in MoS₂ Nanoclusters. *Nanotechnology* 2003, 14, 385.
- (56) Topsoe, N.; Topsoe, H. FTIR Studies of Mo/Al₂O₃-Based Catalysts: II. Evidence for the Presence of SH Groups and Their Role in Acidity and Activity. J. Catal. 1993, 139, 641–651.
- (57) Ma, K. Y.; Yoon, S. I.; Jang, A.-R.; Jeong, H. Y.; Kim, Y.-J.; Nayak, P. K.; Shin, H. S. Hydrogenation of Monolayer Molybdenum Diselenide via Hydrogen plasma treatment. J. Mater. Chem. C 2017, 5, 11294–11300.
- (58) Din, N. U.; Turkowski, V.; Rahman, T. S. Excited States in Hydrogenated Single-layer MoS₂. Journal of Physics: Condensed Matter **2020**, 33, 075201.
- (59) Pandey, D.; Chakrabarti, A. Prediction of Two-dimensional Monochalcogenides: MoS and WS. *Physics Letters A* **2019**, *383*, 2914–2921.
- (60) Calixto, M.; Romera, E. Inverse Participation Ratio and Localization in Topological Insulator Phase Transitions. J. Stat. Mech.: Theory Exp 2015, 2015, P06029.

- (61) Steenbock, T.; Drescher, E.; Dittmann, T.; Bester, G. How Surface Defects Shape the Excitons and Photoluminescence of Ultrasmall CdSe Quantum Dots. Chem. Mater. 2024, 36, 6504–6514.
- (62) Niebur, A.; Lorenz, T.; Schreiber, M.; Seifert, G.; Gemming, S.; Joswig, J.-O. Localization of Edge States at Triangular Defects in Periodic MoS₂ Monolayers. *Phys. Rev. Mater.* 2021, 5, 064001.
- (63) Niebur, A.; Lorenz, T.; Joswig, J.-O.; Seifert, G.; Gemming, S.; Schreiber, M. Closed-Loop Defect States in 2D Materials with Honeycomb Lattice Structure: Molybdenum Disulfide. Phys. Status Solidi B 2021, 258, 2100214.
- (64) Yuan, Y.-J.; Yu, Z.-T.; Liu, X.-J.; Cai, J.-G.; Guan, Z.-J.; Zou, Z.-G. Hydrogen Photogeneration Promoted by Efficient Electron Transfer from Iridium Sensitizers to Colloidal MoS₂ Catalysts. Sci. Rep. 2014, 4, 4045.
- (65) Kayal, A.; De, M. Organo-Soluble Colloidal MoS2 Quantum Dots (QDs) as an Efficient Photocatalyst for α-Amino Phosphonate Synthesis. ChemCatChem 2024, 16, e202400264.
- (66) Rahman, A.; Jennings, J. R.; Tan, A. L.; Khan, M. M. Molybdenum Disulfide-Based Nanomaterials for Visible-Light-Induced Photocatalysis. ACS Omega 2022, 7, 22089– 22110.
- (67) Li, Z.; Meng, X.; Zhang, Z. Recent Development on MoS₂-based Photocatalysis: A Review. J. Photochem. Photobiol., C 2018, 35, 39–55.
- (68) Yuan, Y.-J.; Lu, H.-W.; Yu, Z.-T.; Zou, Z.-G. Noble-Metal-Free Molybdenum Disulfide Cocatalyst for Photocatalytic Hydrogen Production. *ChemSusChem* **2015**, *8*, 4113–4127.

- (69) Jin, X.; Fan, X.; Tian, J.; Cheng, R.; Li, M.; Zhang, L. MoS₂ Quantum dot Decorated g-C₃N₄ Composite Photocatalyst with Enhanced Hydrogen Evolution Performance. RSC Adv. 2016, 6, 52611–52619.
- (70) Xiao, P.; Lou, J.; Zhang, H.; Song, W.; Wu, X.-L.; Lin, H.; Chen, J.; Liu, S.; Wang, X. Enhanced Visible-light-driven Photocatalysis from WS2 Quantum Dots Coupled to BiOCl Nanosheets: Synergistic Effect and Mechanism Insight. Catal. Sci. Technol. 2018, 8, 201–209.
- (71) Zou, Y.; Shi, J.-W.; Ma, D.; Fan, Z.; Cheng, L.; Sun, D.; Wang, Z.; Niu, C. WS₂/Graphitic Carbon Nitride Heterojunction Nanosheets Decorated with CdS Quantum Dots for Photocatalytic Hydrogen Production. *ChemSusChem* 2018, 11, 1187–1197.

TOC Graphic

